Biomedical Microdevices (2018) 20: 104
https://doi.org/10.1007/s10544-018-0346-9

Flattened fiber-optic ATR sensor enhanced by silver nanoparticles for glucose measurement

Wenwen Li[1] · Changyue Sun[1] · Songlin Yu[2] · Zhihua Pu[1] · Penghao Zhang[1] · Kexin Xu[1] · Zhenqiang Song[3] · Dachao Li[1]

Published online: 23 November 2018

Abstract
This paper proposes a novel fiber attenuated total reflection (ATR) sensor with silver nanoparticles (AgNPs) on the flattened structure based on mid-infrared spectroscopy for detecting low concentration of glucose with high precision. The flattened structure was designed to add the effective optical path length to improve the sensitivity. AgNPs were then deposited on the surface of the flattened area of the fiber via chemical silver mirror reaction for further improving the sensitivity by enhancing the infrared absorption. Combining the AgNPs modified flattened fiber ATR sensor with a CO_2 laser showed a strong mid-infrared glucose absorption, with an enhancement factor of 4.30. The glucose concentration could be obtained by a five-variable partial least-squares model with a root-mean-square error of 4.42 mg/dL, which satisfies clinical requirements. Moreover, the fiber-based technique provides a pretty good method to fabricate miniaturized ATR sensors that are suitable to be integrated into a microfluidic chip for continuous glucose monitoring with high sensitivity.

Keywords Attenuated total reflection sensor · Flattened structure · AgNPs · Mid-infrared spectroscopy · Continuous glucose monitoring

1 Introduction

Diabetes is one of the most common chronic disease which demands continuous glucose monitoring to offer direction for diagnosis and treatment. Nowadays, there are great demand for better detection techniques because of current technologies of glucose in blood which are invasive and painful. It was reported that there is a high correlation between glucose concentrations in interstitial fluid (ISF) and blood (Keenan et al. 2013; Rebrin and Steil 2000; Shi et al. 2016). The continuous glucose monitoring of ISF could be used to detect and correct the abnormal blood glucose. At present, implantable enzyme electrode sensors become the most widely applied way to continuous glucose monitoring in clinic. The most representative products include Paradigm ®Real-Time (Medtronic. Inc) (Mastrototaro et al. 2008), FreeStyle Navigator® (Abbott Laboratories) (Wilson et al. 2007) and SEVEN® Plus (DexCom. Inc) (Bailey et al. 2009). However, due to the influence of human bioelectricity and anoxic environment, the measuring signal of the sensor drifts significantly, which results in (Keenan et al. 2013)the difficulty to obtain accurate measurement values. Moreover, for these implantable biosensors based on enzyme electrode, the local glucose molecules are irreversibly depleted in the enzymatic reaction catalyzed by glucose oxidase, which results in measurement inaccuracy at low glucose concentrations (Cha and Meyerhoff 2017).

In terms of continuous glucose monitoring, the optical attenuated total reflection (ATR) sensor has two advantages compared to the enzyme electrode sensor. Firstly, it works based on optical signal, which avoids the effect of the body's bioelectricity, significantly reduces the signal drift and improves the accuracy. Secondly, five emitted wavelengths nearby the glucose absorption peaks are used for the specific detection instead of the specificity of an enzyme (Cao et al. 2012; Yu et al. 2014b), therefore, there is no glucose depleted during the detection.

✉ Zhenqiang Song
zsong@tmu.edu.cn

✉ Dachao Li
dchli@tju.edu.cn

[1] State Key Laboratory of Precision Measuring Technology and Instruments, Tianjin University, Tianjin, China

[2] Temperature Laboratory, Tianjin Institute of Metrological Supervision Testing, Tianjin, China

[3] NHC Key Laboratory of Hormones and Development (Tianjin Medical University) , Tianjin Key Laboratory of Metabolic Diseases, Tianjin Medical University Metabolic Diseases Hospital & Tianjin Institute of Endocrinology, Tianjin, China

The semi-circular, U-shaped, double-coiled and triple-coiled fiber-optic ATR sensors were reported in our previous work, while the sensors were too large for subcutaneous implantation or integration in a chip(Yu et al. 2014b). In our study, a fiber ATR sensor with silver nanoparticles on the flattened structure is proposed. This flattened structure is suitable for integrating into the microfluidic chip for extracting and collecting of ISF developed in our group(Yu et al. 2012). For improving the sensitivity of the ATR sensor, and further realize the accurate detection of glucose concentration in diluted ISF, silver nanoparticles (AgNPs) were deposited on the flattened structure. The combination of optical fiber and extraction chip not only avoids the injury of fiber implantation, but also is convenient for the in vitro calibration of the sensors, which is very beneficial to the long term continuous glucose monitoring.

2 Materials and methods

2.1 Design of Fiber ATR sensor

The structure of the fiber ATR sensor was designed with the two characteristics: (1) a flattened structure and (2) AgNPs grown on the flattened area. Figure 1a shows the three-dimensional schematic of flattened fiber ATR sensor increased by AgNPs installed on this connector, it was designed into three parts, the symmetrical cylinder called conical area on the either side and the sensitive area of sensor called flattened area. Figure 1b shows local magnification map of the flattened area. The thickness of flattened area was controlled by the pressure on two flat plates and measured by Vernier caliper.

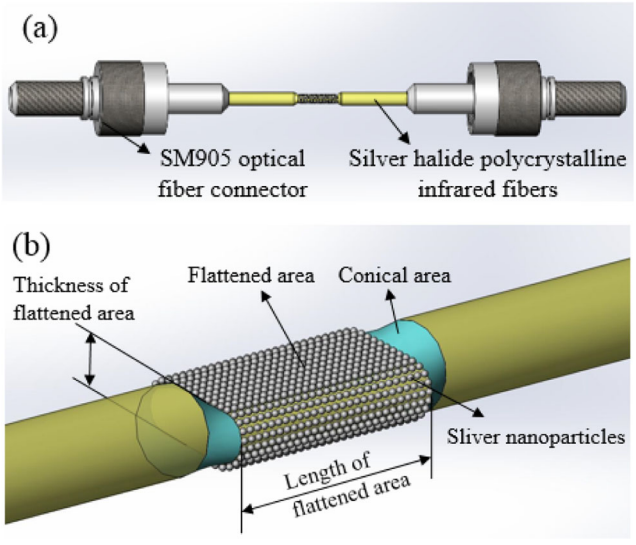

Fig. 1 Schematic of flattened fiber ATR sensor enhanced by AgNPs. (a) The three-dimensional schematic of flattened fiber ATR sensor enhanced by AgNPs installed on the connection head. (b) Local magnification map of the flattened area

The surface roughness of flattened area was measured by step profiler (Alpha-Step IQ from KLA-Tencor) in multiple lateral and longitudinal directions, and the measured surface roughness R_a was within 20~100 nm. The AgNPs were decorated on the surface of the flattened area of the ATR sensor by chemical silver mirror reaction. These two characteristics will improve the sensitivity of fiber ATR sensor by increasing the effective optical path and the infrared absorption, respectively.

2.2 Enhancement mechanisms of Fiber ATR sensor

2.2.1 Enhancement mechanisms of flattened structure

The flattened fiber ATR sensor can enhance the sensitivity by adding the effective optical path length of the flattened area compared to that of a straight fiber ATR sensor. The effective optical path length is determined by the single penetration depth of the evanescent wave and the numbers of total reflection (Raichlin et al. 2003; Yu et al. 2012; Yu et al. 2014b). The single penetration depth and the numbers of total reflection can be expressed as (1) based on reference(Ahmad and Hench 2005):

$$dp = \frac{\lambda_0}{2\pi n_1 \left[\sin^2\theta - (n_2/n_1)^2\right]^{1/2}} \quad (1)$$

$$N = \frac{L}{2d}\cot\theta$$

Where λ_0 represents the light wavelength in a vacuum, θ is the angle of the incident light and the flattened area normal, n_1 and n_2 indicate the refractive index of the fiber core and sample, respectively, L and d are the length and thickness of flattened area of ATR fiber sensor, respectively. In the flattened structure, the incident angle of total reflection becomes smaller, resulting in the greater depth of penetration and the higher total reflection frequency. Furthermore, the smaller thickness of flattened area also leads to the higher total reflection frequency. Accordingly, the sensitivity of the flattened fiber ATR sensor will be higher, when the incident wavelength is longer and the thickness of flattened area is thinner (Raichlin et al. 2014). In this paper, the flattened fiber was conveniently fabricated by a table vise with two 1.5 cm wide plates. By controlling the angle of the handle rotation, the fibers were flattened with different thicknesses of 360 μm, 440 μm, 520 μm and 580 μm. Under the influence of incident wavelength and the thickness of flattened area, the sensitivity of this flattened ATR sensor is studied in the following section.

2.2.2 Enhancement mechanisms of molecular absorption by AgNPs

The ATR sensor with AgNPs on the flattened area has higher infrared absorption mainly due to its electromagnetic and

chemical mechanisms. The following is the expression of infrared absorption (Osawa 2001).

$$A \propto |\partial \mu / \partial Q \cdot \mathrm{E}|^2 = |\partial \mu / \partial Q|^2 |\mathrm{E}|^2 \cos^2 \theta \quad (2)$$

Where $\partial\mu/\partial Q$ is the differential coefficient of molecular dipole moments to the coordinate Q, E is the original vibratory electric field of the excited silver molecules, θ represents the included angle between $\partial\mu/\partial Q$ and E. The electromagnetic enhancement mechanism states that the field intensity generated by incident light is coupled with the metal surface, and the local electric field (E) on the AgNPs has an increase (Hartstein et al. 1980; Osawa 1997). However, the chemical enhancement mechanism states that the absorption coefficient (i.e.,$|\partial\mu/\partial Q|^2$) of molecules has an increase because of the chemical reactions of the absorbed glucose molecules and the AgNPs (Dumas et al. 1986; Merklin and Griffiths 1997). Consequently, the increase of infrared absorption is the synergistic effect of its electromagnetic and chemical mechanisms.

2.3 Fabrication of AgNPs on the flattened surface of Fiber ATR sensor

2.3.1 Growing method of the AgNPs

Vacuum evaporation (Khedmi et al. 2014; Lu et al. 2014) and sputtering (Delgado et al. 2008; Verger et al. 2012) both are major dry processes to grow nanoparticles, however, they cannot easily be applied to simultaneously growing nanoparticles on both sides of a flat substrate. Wet chemical processes has the advantages of lower cost and easier preparation (Chang and Yang 2010; Lopez-Lorente et al. 2014; Rao and Yang 2011). Most importantly, they can grow AgNPs on the two sides of flat substrates simultaneously. Chemical silver mirror reaction is a wet chemical method that has the advantages of simple, high reproducibility, and effective in preparing AgNPs (von Lilienfeld-Toal et al. 2005). The common silver mirror reaction produces an Ag film. To acquire AgNPs, ethanol was added as a dispersing agent of the silver mirror reaction. In the chemical silver mirror reaction, silver ions are reduced by glucose that acts as a reducing agent as shown in the following equations.

$$\begin{aligned} &AgNO_3 + NH_3 \cdot H_2O \rightarrow NH_4NO_3 + AgOH2AgOH \rightarrow Ag_2O + H_2OAg_2O \\ &+ 4NH_3 \cdot H_2O \rightarrow 2\left[Ag(NH_3)_2\right]OH + 3H_2OCH_2OH(CHOH)_4CHO \\ &+ 2\left[Ag(NH_3)_2\right]OH \rightarrow CH_2OH(CHOH)_4COONH_4 + 2Ag\downarrow + 3NH_3 + H_2O \end{aligned} \quad (3)$$

The AgNPs would be deposited on the spot of fiber ATR sensors that are immersed into the reaction solution. The morphology of AgNPs was changed by adjusting reaction conditions, and then we measured it by scanning electron microscopy (SEM).

2.3.2 Fabrication procedures of the AgNPs

All glassware was cleaned (ethanol, peroxide, deionized water), subjected to ultrasound (15 min), and then dried (70 °C for 30 min). Ammonia (2%) was poured slowly into different concentrations of silver nitrate solution (0.5%, 1%, 1.5%, and 2%) to obtain different concentrations of silver ammonia solution. A little sodium hydroxide was dropped into solution for adjusting the PH value to 10. Then, glucose (10%) was poured into the silver ammonia solution at a dose depending upon the concentration of silver nitrate. This sensor was then put into the solution, and the reaction temperature (60 °C) could be adjusted by a water bath. When the specified reaction time(30 s, 60 s, 90 s) was reached, the sensor was taken out of the solution, and then completely covered with deionized water for 2 min in order to stop the reaction. Then, soluble particles could be cleaned completely by deionized water. The morphology of AgNPs on the fiber ATR sensor was investigated using a scanning electron microscope (S-4800, Hitachi, Japan). Due to the low photostability of the silver halide fiber, all the experimental procedures were carried out in a dark room.

2.3.3 Effectiveness of different growing conditions on the surface morphology of the AgNPs

During the deposition process of the AgNPs on the surface of this sensor, the size, shape and distribution of AgNPs could be adjusted by different conditions, including the silver nitrate concentration and reaction time, and these will ultimately influence the absorption signals of glucose. In order to simplify the descriptions of the reaction conditions, they are denoted using the notation P^xt^k, where P represents the silver nitrate concentration of x% and t is the reaction time of k seconds. $P^{1\%}t^{60}$ represents a AgNPs modified fiber ATR sensor which the preparation conditions are 1% silver nitrate and the reaction time of 60 s, for instance. The preliminarily evaluation results that the size and distribution of the AgNPs growing on the surface of the fiber ATR sensor was obtained by a SEM, and the images are shown in Figs. 2 and 3.

Figure 2 shows that the size of AgNPs is larger for higher silver nitrate concentration. If the concentration of silver nitrate in this reaction is too low, the AgNPs will not be formed due to the rare silver ions. So the AgNPs (as shown in Fig. 2a) are very small (30–40 nm) and few if the concentration of silver nitrate is only 0.5%. The silver nitrate concentration is required to be increased to narrow the inter-particle gaps, as the enhancement of absorption decreases with the increase of inter-particle gap (Verger et al. 2012). If the concentration of silver nitrate has been increased to over 1.5%, the AgNPs begin to aggregate into larger clusters with the size of more than 80 nm and up to 150 nm. The aggregated nanoparticles could cause distortions in absorption bands and influence

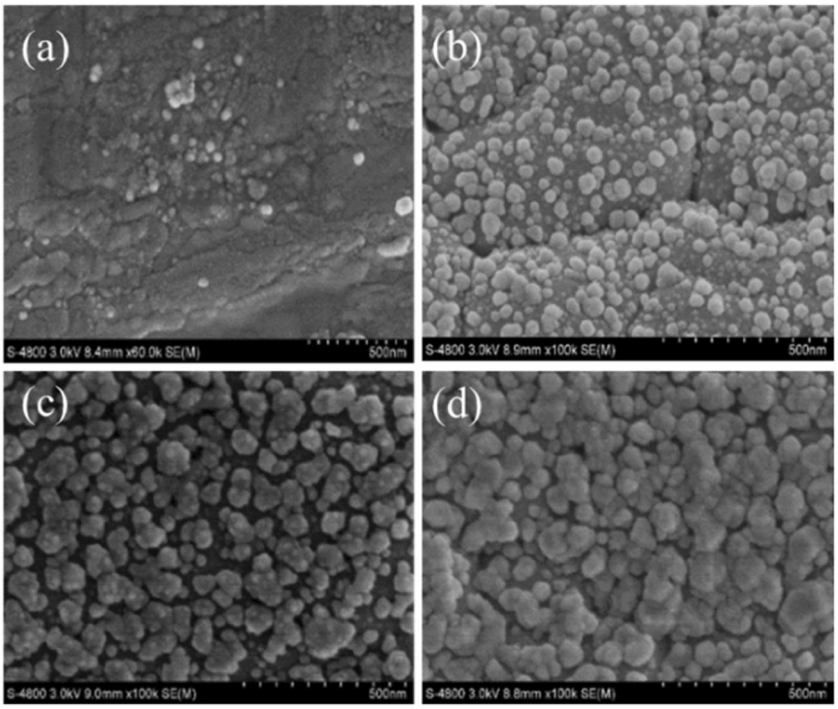

Fig. 2 Effect of silver nitrate concentration (**a**) $P^{0.5\%}t^{60}$, (**b**) $P^{1\%}t^{60}$, (**c**) $P^{1.5\%}t^{60}$, (**d**) $P^{2\%}t^{60}$

their enhancement effect. If the concentration of silver nitrate is reached to 1%, the formed AgNPs in this reaction are uniform with the size of about 50 nm. The uniform distribution of AgNPs without aggregation is better for absorption enhancement.

Figure 3 shows that the AgNPs begin to aggregate gradually on the circumferential surface of the fiber as the reaction time increases. When the reaction time is 30 s, the AgNPs scatters thinly over the surface with the size of about 30 nm. When the reaction time is increased to 90 s, the AgNPs begin to aggregate. The aforementioned results shows that the AgNPs are not only even and about 50 nm, but also few clusters at the condition of $P^{1\%}t^{60}$. Both of higher silver nitrate concentration and longer reaction time can make the AgNPs more easily to form, but it is not favorable to obtain a large increase of the mid-infrared glucose absorption, the $P^{1\%}t^{60}$ as the optimum conditions for the deposition of AgNPs was chosen.

2.3.4 Reproducibility of AgNPs grown via chemical silver mirror reaction

There are many difficulties in controlling the characteristics of the AgNPs using chemical deposition. So, we conducted many experiments to solve the problem. Ultimately, uniform AgNPs (approximately 50 nm and few clusters) could be obtained under the optimum deposition conditions ($P^{1\%}t^{60}$) by the chemical deposition method. From the Fig. 4, we can see the morphologies of the AgNPs on the two different fibers are similar, which indicates the superior reproducibility of AgNPs grown by chemical deposition.

3 References and discussion

3.1 Simulation of the flattened Fiber ATR sensor

3.1.1 Effectiveness of wavenumber on the absorbance of glucose

Figure 5 depicts the absorbance variation curve of glucose solution on the flattened fiber ATR sensor with different incident wavelengths (9.250 μm, 9.293 μm, 9.524 μm, 9.606 μm, 9.643 μm). The thickness and length of the flattened area were 440 μm and 1.5 cm, respectively.

When the glucose concentration is changed by δC, the absorbance of the fiber ATR sensor is changed by δA, accordingly, the sensitivity can be expressed as (4).

$$S_n = \frac{\delta A}{\delta C} \tag{4}$$

The sensitivity values of this ATR sensor with different wavenumbers of 1081, 1076, 1051, 1041 and 1037 cm^{-1} were 0.0042, 0.00422, 0.00432, 0.00438 and 0.00481 respectively. The sensitivity of the sensor is improved as the incident wavenumber decreases in a small degree. For mid-infrared spectrum, the absorption intensity in long-wave band is enhanced by the increase in the penetration depth of the evanescent wave, while it was relatively weak in short-wave band. As shown in Fig. 5, the absorbance slightly increased as the incident wavenumber decreased, which corresponds with the characteristic of the mid-infrared spectrum.

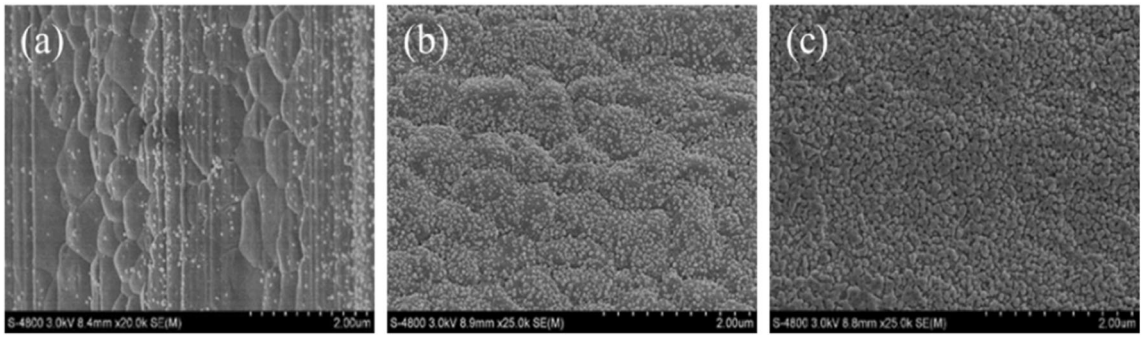

Fig. 3 Effect of deposition time (**a**) $P^{1\%}t^{30}$, (**b**) $P^{1\%}t^{60}$, (**c**) $P^{1\%}t^{90}$

3.1.2 Effectiveness of the thickness of the flattened area on the absorbance of glucose

The absorbance of glucose for fiber ATR sensors with different thicknesses (580 μm, 520 μm, 440 μm, 360 μm) at wavenumber of 1037 cm^{-1} is shown in Fig. 6. The length of the flattened area of the fiber ATR sensor was 1.5 cm.

As the thickness of the flattened area decreases, the sensitivity of the sensor gradually increases, indicating that the thickness of the flattened area has an important influence on the sensitivity of the sensor. One important thing to note is that the sensor would be easy to break when the flattened area was too thin, even though it could obtain the higher sensitivity. Therefore, 440 μm was selected as the optimal thickness for the flattened area of the flattened fiber ATR sensor according to the simulation result.

3.2 Experimental measurement system

The fiber ATR sensor can realize the optical detection of glucose spectrum in the mid-infrared band. In this paper, the system applied five wavelengths nearby the two strong glucose absorption peaks that were radiated from the wavelength-tunable CO_2 laser(customized from Access Laser Co. in Washington, USA) to eliminate the effects of large biological molecules in the ISF for the detection of glucose (Damm et al. 2007; Heise et al. 2001; Pleitez et al. 2012).

Because of the operation principle of the CO_2 laser, there are many difficulties to adjust the working wavenumber, meanwhile, make the line frequency and power stably, although these parameters are important to the accurate detection of glucose concentration. The emission wavelengths could be tuned using a stepping motor by rotating an optical grating. Moreover, there are stable line frequency and power by a photoelectric detection feedback mechanism in the experimental system, and tunable cavity length with a micro piezoelectric actuator (Yu et al. 2014b). In our research, the CO_2 laser can realize line tuning in the range of 9.19–9.77 μm. Five emitted wavelengths nearby the glucose absorption peaks 9.259 μm and 9.662 μm, including 9.250, 9.293, 9.524, 9.606, 9.643 μm, were chosen as working wavelengths for the specific glucose detection (Lu et al. 2014), and the five wavelengths around the two absorption

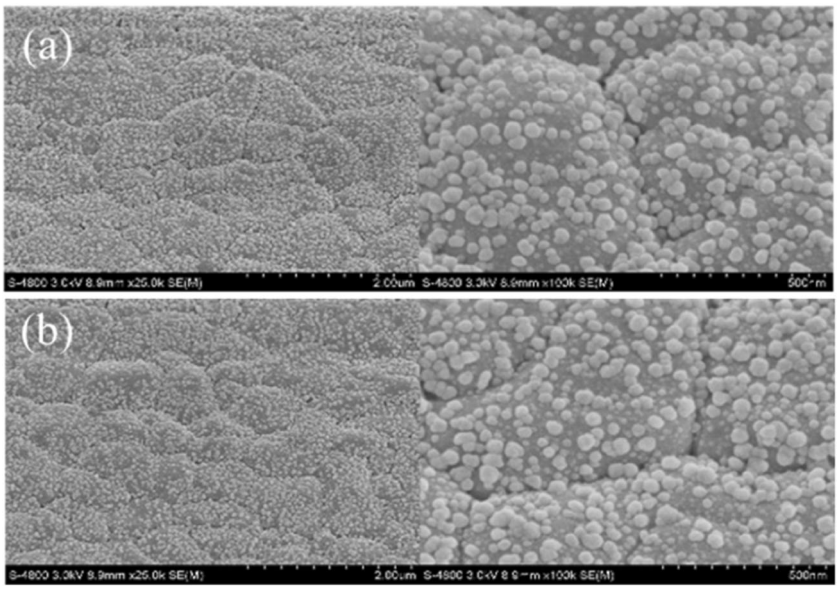

Fig. 4 Morphologies of the AgNPs on two different silver halide infrared fibers

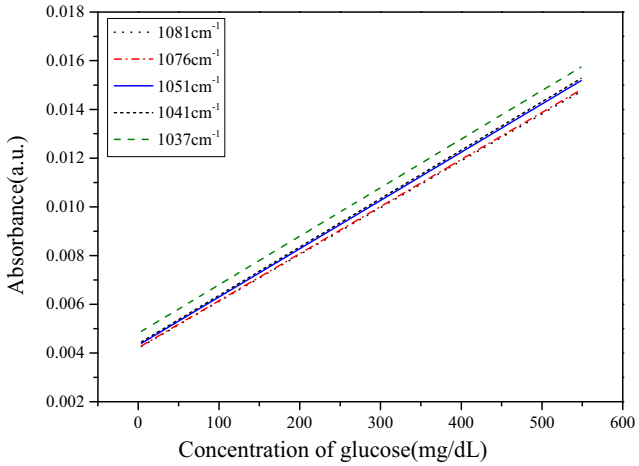

Fig. 5 Plot of absorbance vs. glucose concentration at different incident wavenumbers

peaks is tunable randomly. All of the operations could be completed by the control panel of LabVIEW software installed on our working computer.

After growing the AgNPs on the optimal condition, the ATR sensor was characterized by glucose solutions (5–500 mg/dL). As demonstrated in Fig. 7, the dual path laser measurement system, which included a tunable CO_2 laser, the proposed sensor and some other basic optical components, was built for glucose detection. An infrared attenuator (Model 401, Lasnix, Germany) was employed to decay the laser output to a feasible level. This decayed laser beam was then separated into two paths, one reference optical path and one sensing path, by ZnSe beam splitter. Incident laser beam of each path was coupled into reference and sensing detectors (Det. R and Det. S). Two lock-in amplifiers (SR830, Stanford Research Systems, Inc., USA) were connected with two infrared detectors (LME-353, InfraTec GmbH, Germany), and the RF circuit provided the synchronized reference frequency (750 Hz). Then, the signals of the two paths were synchronously collected via the data acquisition card. All of these operations were controlled by a control board with LabView software installed on a computer.

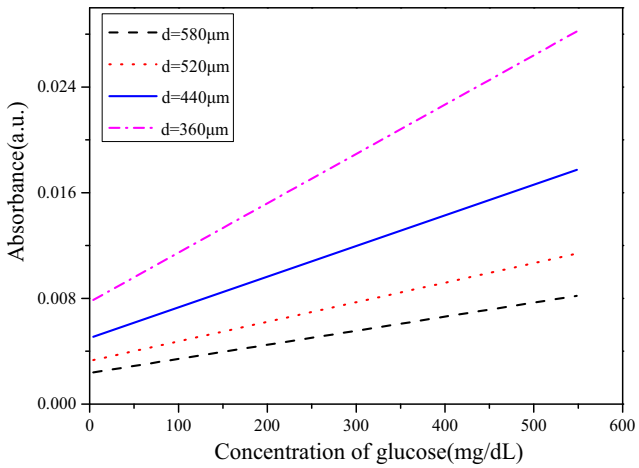

Fig. 6 Plot of absorbance vs. glucose concentration for different thicknesses of the flattened area

The absorbance changed with glucose concentration variation is expressed as (5):

$$A_s = \ln\left(u_b^s/u_g^s\right) + \ln\left(u_g^r/u_b^r\right) \quad (5)$$

Where u is the lock-in amplified voltage, superscripts "s" and "r" are the sensing and reference paths, respectively, and subscripts "b" and "g" represent the background and glucose solutions, respectively. To test the effect of the AgNPs, the flattened ATR sensor without AgNPs was used as a reference. For the experiment, water was acted as not only the sample but also background solution, and the five tuning wavelengths were applied for recording the transmission intensity of each solution.

3.3 Effectiveness of the flattened area on glucose absorbance

Using the two path laser measurement device, the glucose absorbance of the fiber ATR sensor with different thicknesses of the flattened area at wavenumber of 1037 cm^{-1} was detected. The approximate trend can be acquired from Fig. 8.

As shown in Fig. 8, the sensitivity of the flattened fiber ATR sensor for glucose concentration measurement increases gradually with the decrease of the thickness of the flattened area. This phenomenon is in accordance with the simulation result. Balancing between the sensitivity and durability of the flattened fiber ATR sensor, 440 μm was chosen as the optimal thickness of flattened area of the fiber ATR sensor.

3.4 Effectiveness of AgNPs on the flattened Fiber ATR sensor

To test the effect of AgNPs on the flattened fiber ATR sensor for glucose detection, flattened (thickness: 440 μm) ATR sensors with and without AgNPs were used to measure the glucose concentration ranging from 15 to 500 mg/dL. AgNPs were deposited on the flattened area of ATR sensors under the optimal deposition condition of $P^{1\%}t^{60}$. The measurement results using the incident wavenumber of 1037 cm^{-1} are shown in Fig. 9. To evaluate the effect of AgNPs, we define the enhancement ratio as the proportion of the absorbance obtained by the flattened fiber ATR sensor with and without AgNPs for the same glucose concentration. The enhancement factor of the flattened fiber ATR sensor increased using AgNPs was 4.30. The sensitivity of the flattened fiber ATR sensors improved greatly by growing AgNPs on the flattened area of the sensor, which provides good direction for the application of the fiber ATR sensors.

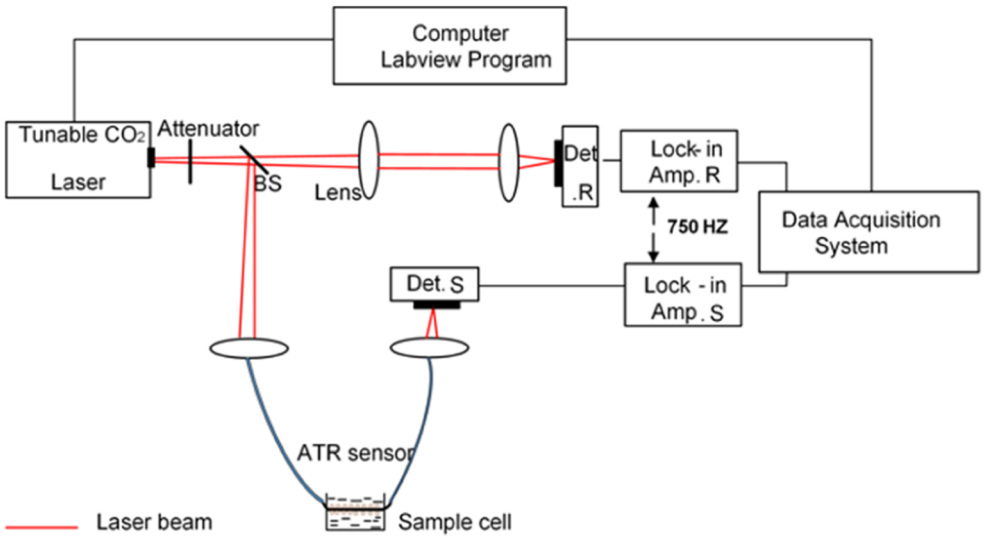

Fig. 7 Schematic of the dual path laser measurement system

3.5 Evaluation of Fiber ATR sensor for glucose measurement

We use a partial least-squares (PLS) (Rosipal and Kramer 2006) algorithm to calibrate the spectral data of five wavelengths, and the PLS model was optimized by a cross-validation. According to the spectral analysis, only one wavenumber cannot be sufficient to identify the analyte. When a discrete wavenumber spectrometer is used, we need at least 3–5 work wavenumbers to determine an analyte and make sure the stability of the prediction model. The prediction quality of the PLS model was evaluated by the root-mean-square error of prediction (RMSEP) and the correlation coefficient (R). The measurement results of the fiber ATR sensor with 440 μm thickness of the flattened area was analyzed by the five-wavelength PLS model.

Figure 10 shows the relationship between the reference and predicted concentration of glucose. The correlation coefficient of the flattened fiber ATR sensor without and with AgNPs were 0.9946 and 0.9996, respectively. Moreover, the RMSEP of the flattened fiber ATR sensor increased using AgNPs was 4.42 mg/dL, which is less than 4.5 mg/dL (Yu et al. 2014a). These results indicate that the prediction accuracy of the sensor increased using AgNPs was higher. This also proves that the flattened fiber ATR sensors increased using AgNPs have a better prospect for clinical application.

4 Integration of the glucose sensor into the ISF extraction chip

MEMS technology is used for producing devices for transdermal ISF extraction, however, the integration of transdermal

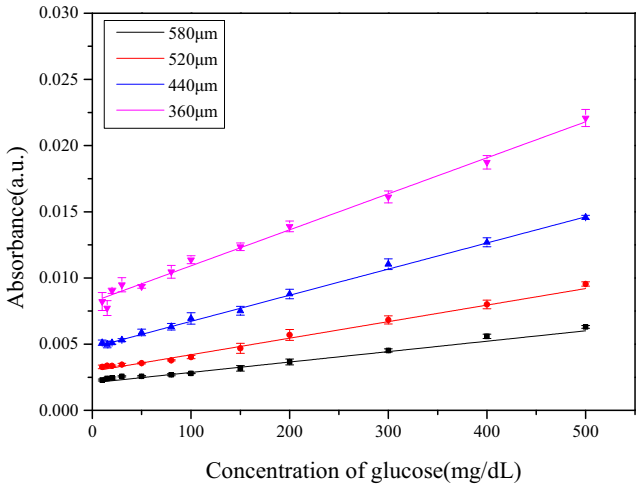

Fig. 8 Plot of absorbance for different thicknesses of the flattened area of the flattened fiber ATR sensor

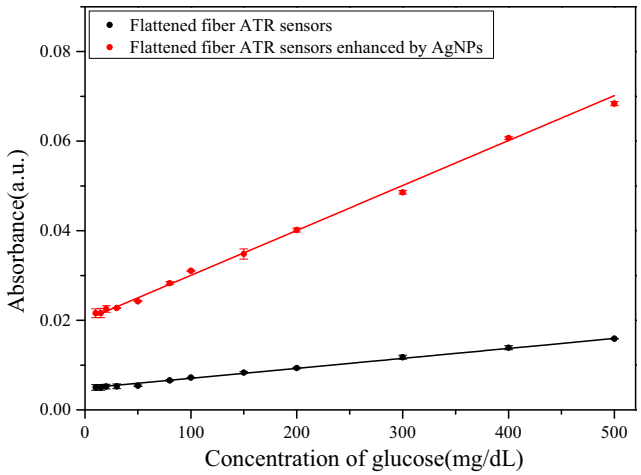

Fig. 9 Plot of glucose absorbance of the flattened fiber ATR sensor with and without AgNPs

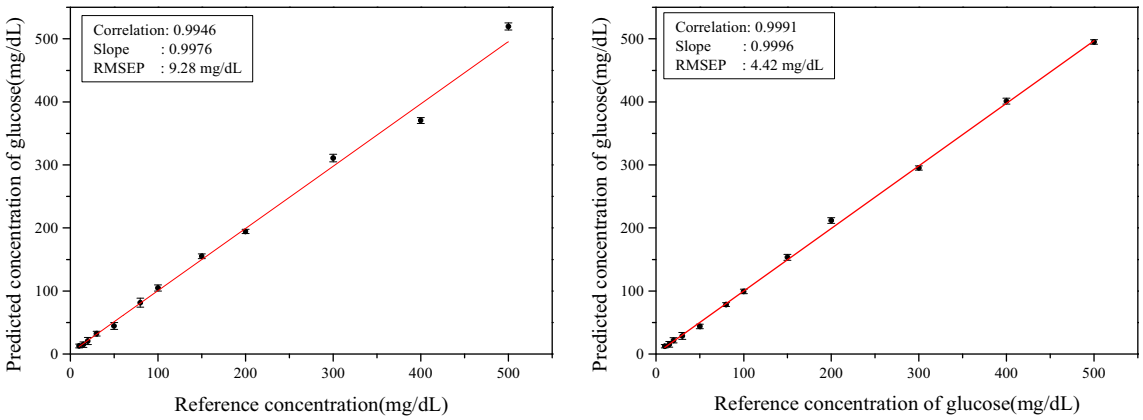

Fig. 10 Prediction of glucose concentration using the five-wavelength PLS model based on the measurement results from (**a**) flattened ATR sensor without AgNPs and (**b**) flattened ATR sensor enhanced by AgNPs

ISF extraction and glucose sensing within one MEMS equipment is not yet mature. An image of the lab-on-a-chip system, which includes a microfluidic chip for ISF extraction and volume measurement as well as a fiber ATR sensor for glucose concentration detection, is shown in Fig. 11. This figure demonstrates the integration ability of the proposed ATR sensor into the microfluidic chip in this investigation. The microfluidic chip is composed of a Venturi to supply driving force for ISF extraction and fluid manipulation, pneumatic valves to control the fluid flow direction in the chip, electrodes to detect the fluid position, and interconnecting micro channels. Besides, negative pressure was provided by a pressure pump connected with Venturi.

A volume sensor composed of the electrode pairs E1-E4 and the S-shape microchannel was used for controlling the input quantity of normal saline, which is stored in the normal saline chamber (diameter: 2 mm) and demanded to mix with transdermally extracted ISF in the extraction chamber (diameter: 3 mm). Then we measured the volume of diluted ISF again by the volume sensor in order to obtain the volume of transdermally extracted ISF. After extracting and diluting the ISF in the microfluidic chip, we transported the ISF to the fiber ATR sensor inside the microchannel. Then the glucose concentration of the diluted ISF is detected by the ATR sensor. The glucose concentration in ISF could be obtained by this measured glucose concentration and volume of the diluted ISF as well as the defined input volume of normal saline. The sensors with U-shaped, double-coiled and triple coiled configurations are difficulty to be integrated into microfluidic chips. However, the proposed ATR sensor can be integrated in a miniaturized, portable system for clinical application, which is another important advantage of our designed sensors. The integration between the microfluidic chip and the designed glucose sensor can be used for transdermally extracting, diluting, collecting ISF, and detecting glucose in ISF, which enables us to develop a device for continuous glucose monitoring.

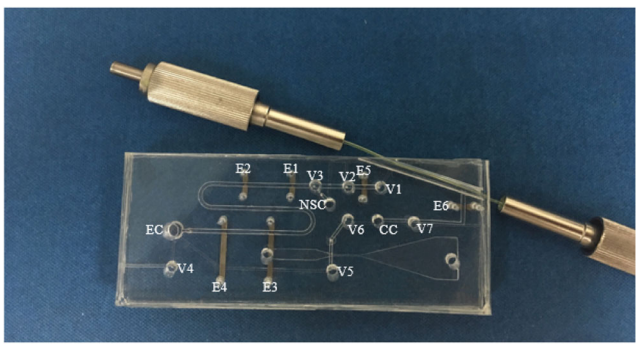

Fig. 11 Image of the lab-on-a–chip system for continuous glucose monitoring. V1-V7 are pneumatic valves. E1-E6 are six pairs of electrodes. EC: Extraction Chamber, NSC: Normal Saline Chamber, CC: Collection Chamber

5 Conclusions

In this paper, a flattened fiber ATR sensor enhanced by AgNPs was proposed to reduce signal drift, meanwhile, it can also solve the problem of hypoglycemia measurement in comparison with the widely used enzyme-electrode sensing technology. To address the issue of the low sensitivity of the miniaturized fiber sensor, we adopt two methods: a flattened structure and growing AgNPs on the flattened area of the fiber sensor. The optimized thickness of the flattened structure was 440 μm. The optimized conditions for growing AgNPs were 1% silver nitrate and the reaction time of 60 s, producing uniformly distributed AgNPs of uniform size of approximately 50 nm, yielding a large enhancement of mid-infrared glucose absorption. A two-path laser detection device was built for glucose measurement by a tunable CO_2 laser and a fiber ATR sensor. The experimental results show that the enhancement factor of the flattened ATR sensor modified by AgNPs was 4.30. The optimal predicted result of glucose level was realized by the five-variable partial least-squares model, and we obtained the result that the root-mean-square error of the

predicted glucose concentration was 4.42 mg/dL, thus indicating the potential of the designed ATR sensor for glucose determination. In addition, the ATR sensor was integrated into an ISF extraction microfluidic chip to combine with the ISF extraction, dilution, and collection for continuous glucose monitoring. Future efforts will be concentrated on applying the flattened ATR sensor with AgNPs integrated into the microfluidic chip for clinical experiment.

Funding This work was supported by the National Natural Science Foundation of China (No.81571766), the National Key Research and Development Program of China (No.2017YFA0205103), and the 111 Project of China (No.B07014).

Compliance with ethical standards

Conflicts of interest The authors declare that there are no conflicts of interest related to this article.

References

M. Ahmad, L.L. Hench, Effect of taper geometries and launch angle on evanescent wave penetration depth in optical fibers. Biosens. Bioelectron. **20**(7), 1312–1319 (2005)

T. Bailey, H. Zisser, A. Chang, New features and performance of a next-generation SEVEN-day continuous glucose monitoring system with short lag time. Diabetes Technol The **11**(12), 749–755 (2009)

Y.Z. Cao, W. Zhang, R. Liu, W.J. Zhang, K.X. Xu, Study of specificity for noninvasive glucose measurements based on two-dimensional correlation mid-infrared spectroscopy. Proc. SPIE **8229** (2012)

K.H. Cha, M.E. Meyerhoff, Compatibility of nitric oxide release with implantable enzymatic glucose sensors based on osmium (III/II) mediated electrochemistry. ACS Sens. **2**(9), 1262–1266 (2017)

R.L.J. Chang, J. Yang, Surface-controlled Electroless deposition method in the preparation of stacked silver nanoparticles on germanium for surface-enhanced infrared absorption measurements. Appl. Spectrosc. **64**(2), 211–218 (2010)

U. Damm, V.R. Kondepati, H.M. Heise, Continuous reagent-free bedside monitoring of glucose in biofluids using infrared spectrometry and micro-dialysis. Vib. Spectrosc. **43**(1), 184–192 (2007)

J.M. Delgado, J.M. Orts, J.M. Perez, A. Rodes, Sputtered thin-film gold electrodes for *in situ* ATR-SEIRAS and SERS studies. J. Electroanal. Chem. **617**(2), 130–140 (2008)

P. Dumas, R.G. Tobin, P.L. Richards, Study of adsorption states and interactions of CO on evaporated noble metal surfaces by infrared absorption spectroscopy. II. Gold and copper. Surface Science **171**(3), 579–599 (1986)

A. Hartstein, J.R. Kirtley, J.C. Tsang, Enhancement of the infrared absorption from molecular monolayers with thin metal overlayers. Phys. Rev. Lett. **45**(3), 201–204 (1980)

H.M. Heise, G. Voigt, P. Lampen, L. Kupper, S. Rudloff, G. Werner, Multivariate calibration for the determination of analytes in urine using mid-infrared attenuated total reflection spectroscopy. Appl. Spectrosc. **55**(4), 434–443 (2001)

D.B. Keenan, J.J. Mastrototaro, S.A. Weinzimer, G.M. Steil, Interstitial fluid glucose time-lag correction for real-time continuous glucose monitoring. Biomed Signal Proces **8**(1), 81–89 (2013)

N. Khedmi, M. Ben Rabeh, M. Kanzari, Structural morphological and optical properties of SnSb2S4 thin films grown by vacuum evaporation method. J. Mater. Sci. Technol. **30**(10), 1006–1011 (2014)

H. von Lilienfeld-Toal, M. Weidenmuller, A. Xhelaj, W. Mantele, A novel approach to non-invasive glucose measurement by mid-infrared spectroscopy: The combination of quantum cascade lasers (QCL) and photoacoustic detection. Vib. Spectrosc. **38**(1–2), 209–215 (2005)

A.I. Lopez-Lorente, M. Sieger, M. Valcarcel, B. Mizaikoff, Infrared attenuated total reflection spectroscopy for the characterization of gold nanoparticles in solution. Anal. Chem. **86**(1), 783–789 (2014)

C. Lu, L. Xingbo, L. Yang, Study of influencing factors on vacuum evaporation film thickness. Appl. Mech. Mater. **536-537**, 3716–3720 (2014)

J. Mastrototaro, J. Shin, A. Marcus, G. Sulur, S.C.T. Investigator, The accuracy and efficacy of real-time continuous glucose monitoring sensor in patients with type 1 diabetes. Diabetes Technol The **10**(5), 385–390 (2008)

G.T. Merklin, P.R. Griffiths, Influence of chemical interactions on the surface-enhanced infrared absorption spectrometry of nitrophenols on copper and silver films. Langmuir **13**(23), 6159–6163 (1997)

M. Osawa, Dynamic processes in electrochemical reactions studied by surface-@enhanced infrared absorption spectroscopy (SEIRAS). Bull. Chem. Soc. Jpn. **70**(12), 2861–2861 (1997)

M. Osawa, in *Near-Field Optics and Surface Plasmon Polaritons*, ed. by S. Kawata. Surface-enhanced infrared absorption (Springer Berlin Heidelberg, Berlin, Heidelberg, 2001), pp. 163–187

M. Pleitez, H. von Lilienfeld-Toal, W. Mantele, Infrared spectroscopic analysis of human interstitial fluid *in vitro* and *in vivo* using FT-IR spectroscopy and pulsed quantum cascade lasers (QCL): Establishing a new approach to non invasive glucose measurement. Spectrochim. Acta A **85**(1), 61–65 (2012)

Y. Raichlin, L. Fel, A. Katzir, Evanescent-wave infrared spectroscopy with flattened fibers as sensing elements. Opt. Lett. **28**(23), 2297–2299 (2003)

Y. Raichlin, D. Avisar, L. Gerber, A. Katzir, Flattened infrared fiber-optic sensors for the analysis of micrograms of insoluble solid particles in solution or in a dry state. Vib. Spectrosc. **73**, 67–72 (2014)

G.P.C. Rao, J. Yang, Preparation of high-capacity substrates from polycrystalline silver chloride for the selective detection of tyrosine by surface-enhanced infrared absorption (SEIRA) measurements. Anal. Bioanal. Chem. **401**(9), 2935–2943 (2011)

K. Rebrin, G.M. Steil, Can interstitial glucose assessment replace blood glucose measurements? Diabetes Technol The **2**(3), 461–472 (2000)

R. Rosipal, N. Kramer, Overview and recent advances in partial least squares. Lect Notes Comput Sc **3940**, 34–51 (2006)

T. Shi, D. Li, G. Li, Y. Zhang, K. Xu, L. Lu, Modeling and measurement of correlation between blood and interstitial glucose changes. Journal of diabetes research **2016**, 1 (2016)

F. Verger, T. Pain, V. Nazabal, C. Boussard-Pledel, B. Bureau, F. Colas, E. Rinnert, K. Boukerma, C. Compere, M. Guilloux-Viry, S. Deputier, A. Perrin, J.P. Guin, Surface enhanced infrared absorption (SEIRA) spectroscopy using gold nanoparticles on As2S3 glass. Sensor Actuat B-Chem **175**, 142–148 (2012)

D.M. Wilson, R.W. Beck, W.V. Tamborlane, M.J. Dontchev, C. Kollman, P. Chase, L.A. Fox, K.J. Ruedy, E. Tsalikian, S.A. Weinzimer, The accuracy of the FreeStyle navigator continuous glucose monitoring system in children with type 1 diabetes. Diabetes Care **30**(1), 59–64 (2007)

H.X. Yu, D.C. Li, R.C. Roberts, K.X. Xu, N.C. Tien, An interstitial fluid transdermal extraction system for continuous glucose monitoring. J Microelectromech S **21**(4), 917–925 (2012)

S.L. Yu, D.C. Li, H. Chong, C.Y. Sun, K.X. Xu, Continuous glucose determination using fiber-based tunable mid-infrared laser spectroscopy. Opt Laser Eng **55**, 78–83 (2014a)

S.L. Yu, D.C. Li, H. Chong, C.Y. Sun, H.X. Yu, K.X. Xu, *In vitro* glucose measurement using tunable mid-infrared laser spectroscopy combined with fiber-optic sensor. Biomed Opt Express **5**(1), 275–286 (2014b)